Observation of Strong Nuclear Suppression in Exclusive J/ψ Photoproduction in Au + Au Ultraperipheral Collisions at RHIC

M. I. Abdulhamid,[4] B. E. Aboona,[56] J. Adam,[16] L. Adamczyk,[2] J. R. Adams,[41] I. Aggarwal,[43] M. M. Aggarwal,[43] Z. Ahammed,[63] E. C. Aschenauer,[6] S. Aslam,[28] J. Atchison,[1] V. Bairathi,[54] J. G. Ball Cap,[24] K. Barish,[11] R. Bellwied,[24] P. Bhagat,[31] A. Bhasin,[31] S. Bhatta,[53] S. R. Bhosale,[19] J. Bielcik,[16] J. Bielcikova,[40] J. D. Brandenburg,[41] C. Broodo,[24] X. Z. Cai,[51] H. Caines,[67] M. Calderón de la Barca Sánchez,[9] D. Cebra,[9] J. Ceska,[16] I. Chakaberia,[34] P. Chaloupka,[16] B. K. Chan,[10] Z. Chang,[29] A. Chatterjee,[18] D. Chen,[11] J. Chen,[50] J. H. Chen,[21] Z. Chen,[50] J. Cheng,[58] Y. Cheng,[10] S. Choudhury,[21] W. Christie,[6] X. Chu,[6] H. J. Crawford,[8] M. Csanád,[19] G. Dale-Gau,[13] A. Das,[16] I. M. Deppner,[23] A. Dhamija,[43] P. Dixit,[26] X. Dong,[34] J. L. Drachenberg,[1] E. Duckworth,[32] J. C. Dunlop,[6] J. Engelage,[8] G. Eppley,[45] S. Esumi,[59] O. Evdokimov,[13] O. Eyser,[6] R. Fatemi,[33] S. Fazio,[7] C. J. Feng,[39] Y. Feng,[44] E. Finch,[52] Y. Fisyak,[6] F. A. Flor,[67] C. Fu,[30] C. A. Gagliardi,[56] T. Galatyuk,[17] T. Gao,[50] F. Geurts,[45] N. Ghimire,[55] A. Gibson,[62] K. Gopal,[27] X. Gou,[50] D. Grosnick,[62] A. Gupta,[31] W. Guryn,[6] A. Hamed,[4] Y. Han,[45] S. Harabasz,[17] M. D. Harasty,[9] J. W. Harris,[67] H. Harrison-Smith,[33] W. He,[21] X. H. He,[30] Y. He,[50] N. Herrmann,[23] L. Holub,[16] C. Hu,[60] Q. Hu,[30] Y. Hu,[34] H. Huang,[39] H. Z. Huang,[10] S. L. Huang,[53] T. Huang,[13] X. Huang,[58] Y. Huang,[58] Y. Huang,[12] T. J. Humanic,[41] M. Isshiki,[59] W. W. Jacobs,[29] A. Jalotra,[31] C. Jena,[27] A. Jentsch,[6] Y. Ji,[34] J. Jia,[6,53] C. Jin,[45] X. Ju,[47] E. G. Judd,[8] S. Kabana,[54] D. Kalinkin,[33] K. Kang,[58] D. Kapukchyan,[11] K. Kauder,[6] D. Keane,[32] A. Khanal,[65] Y. V. Khyzhniak,[41] D. P. Kikoła,[64] D. Kincses,[19] I. Kisel,[20] A. Kiselev,[6] A. G. Knospe,[35] H. S. Ko,[34] L. K. Kosarzewski,[41] L. Kumar,[43] M. C. Labonte,[9] R. Lacey,[53] J. M. Landgraf,[6] J. Lauret,[6] A. Lebedev,[6] J. H. Lee,[6] Y. H. Leung,[23] N. Lewis,[6] C. Li,[50] D. Li,[47] H-S. Li,[44] H. Li,[66] W. Li,[45] X. Li,[47] Y. Li,[47] Y. Li,[58] Z. Li,[47] X. Liang,[11] Y. Liang,[32] R. Licenik,[40,16] T. Lin,[50] Y. Lin,[22] M. A. Lisa,[41] C. Liu,[30] G. Liu,[48] H. Liu,[12] L. Liu,[12] T. Liu,[67] X. Liu,[41] Y. Liu,[56] Z. Liu,[12] T. Ljubicic,[45] O. Lomicky,[16] R. S. Longacre,[6] E. M. Loyd,[11] T. Lu,[30] J. Luo,[47] X. F. Luo,[12] L. Ma,[21] R. Ma,[6] Y. G. Ma,[21] N. Magdy,[53] D. Mallick,[64] R. Manikandhan,[24] S. Margetis,[32] C. Markert,[57] G. McNamara,[65] O. Mezhanska,[16] K. Mi,[12] S. Mioduszewski,[56] B. Mohanty,[38] M. M. Mondal,[38] I. Mooney,[67] J. Mrazkova,[40,16] M. I. Nagy,[19] A. S. Nain,[43] J. D. Nam,[55] M. Nasim,[68] D. Neff,[10] J. M. Nelson,[8] D. B. Nemes,[67] M. Nie,[50] G. Nigmatkulov,[13] T. Niida,[59] T. Nonaka,[59] G. Odyniec,[34] A. Ogawa,[6] S. Oh,[49] K. Okubo,[59] B. S. Page,[6] R. Pak,[6] S. Pal,[16] A. Pandav,[34] A. K. Pandey,[30] T. Pani,[46] A. Paul,[11] B. Pawlik,[42] D. Pawlowska,[64] C. Perkins,[8] J. Pluta,[64] B. R. Pokhrel,[55] M. Posik,[55] T. Protzman,[35] V. Prozorova,[16] N. K. Pruthi,[43] M. Przybycien,[2] J. Putschke,[65] Z. Qin,[58] H. Qiu,[30] C. Racz,[11] S. K. Radhakrishnan,[32] A. Rana,[43] R. L. Ray,[57] R. Reed,[35] C. W. Robertson,[44] M. Robotkova,[40,16] M. A. Rosales Aguilar,[33] D. Roy,[46] P. Roy Chowdhury,[64] L. Ruan,[6] A. K. Sahoo,[68] N. R. Sahoo,[27] H. Sako,[59] S. Salur,[46] S. Sato,[59] B. C. Schaefer,[35] W. B. Schmidke,[6,*] N. Schmitz,[36] F-J. Seck,[17] J. Seger,[15] R. Seto,[11] P. Seyboth,[36] N. Shah,[28] P. V. Shanmuganathan,[6] T. Shao,[21] M. Sharma,[31] N. Sharma,[68] R. Sharma,[27] S. R. Sharma,[27] A. I. Sheikh,[32] D. Shen,[50] D. Y. Shen,[21] K. Shen,[47] S. S. Shi,[12] Y. Shi,[50] Q. Y. Shou,[21] F. Si,[47] J. Singh,[43] S. Singha,[30] P. Sinha,[27] M. J. Skoby,[5,44] N. Smirnov,[67] Y. Söhngen,[23] Y. Song,[67] B. Srivastava,[44] T. D. S. Stanislaus,[62] M. Stefaniak,[41] D. J. Stewart,[65] Y. Su,[47] M. Sumbera,[40] C. Sun,[53] X. Sun,[30] Y. Sun,[47] Y. Sun,[25] B. Surrow,[55] M. Svoboda,[40,16] Z. W. Sweger,[9] A. C. Tamis,[67] A. H. Tang,[6] Z. Tang,[47] T. Tarnowsky,[37] J. H. Thomas,[34] A. R. Timmins,[24] D. Tlusty,[15] T. Todoroki,[59] S. Trentalange,[10] P. Tribedy,[6] S. K. Tripathy,[64] T. Truhlar,[16] B. A. Trzeciak,[16] O. D. Tsai,[10,6] C. Y. Tsang,[32,6] Z. Tu,[6] J. Tyler,[56] T. Ullrich,[6] D. G. Underwood,[3,62] I. Upsal,[47] G. Van Buren,[6] J. Vanek,[6] I. Vassiliev,[20] V. Verkest,[65] F. Videbæk,[6] S. A. Voloshin,[65] F. Wang,[44] G. Wang,[10] J. S. Wang,[25] J. Wang,[50] K. Wang,[47] X. Wang,[50] Y. Wang,[47] Y. Wang,[12] Y. Wang,[58] Z. Wang,[50] J. C. Webb,[6] P. C. Weidenkaff,[23] G. D. Westfall,[37] D. Wielanek,[64] H. Wieman,[34] G. Wilks,[13] S. W. Wissink,[29] R. Witt,[61] J. Wu,[12] J. Wu,[30] X. Wu,[10] X. Wu,[47] B. Xi,[21] Z. G. Xiao,[58] G. Xie,[60] W. Xie,[44] H. Xu,[25] N. Xu,[34] Q. H. Xu,[50] Y. Xu,[50] Y. Xu,[12] Z. Xu,[32] Z. Xu,[10] G. Yan,[50] Z. Yan,[53] C. Yang,[50] Q. Yang,[50] S. Yang,[48] Y. Yang,[39] Z. Ye,[45] Z. Ye,[34] L. Yi,[50] K. Yip,[6] Y. Yu,[50] H. Zbroszczyk,[64] W. Zha,[47] C. Zhang,[21] D. Zhang,[48] J. Zhang,[50] S. Zhang,[14] W. Zhang,[48] X. Zhang,[30] Y. Zhang,[30] Y. Zhang,[47] Y. Zhang,[50] Y. Zhang,[12] Z. J. Zhang,[39] Z. Zhang,[6] Z. Zhang,[13] F. Zhao,[30] J. Zhao,[21] M. Zhao,[6] J. Zhou,[47] S. Zhou,[12] Y. Zhou,[12] X. Zhu,[58] M. Zurek,[3,6] and M. Zyzak[20]

(STAR Collaboration)

*Deceased.

052301-1

[1]*Abilene Christian University, Abilene, Texas 79699*
[2]*AGH University of Krakow, FPACS, Cracow 30-059, Poland*
[3]*Argonne National Laboratory, Argonne, Illinois 60439*
[4]*American University in Cairo, New Cairo 11835, Egypt*
[5]*Ball State University, Muncie, Indiana, 47306*
[6]*Brookhaven National Laboratory, Upton, New York 11973*
[7]*University of Calabria & INFN-Cosenza, Rende 87036, Italy*
[8]*University of California, Berkeley, California 94720*
[9]*University of California, Davis, California 95616*
[10]*University of California, Los Angeles, California 90095*
[11]*University of California, Riverside, California 92521*
[12]*Central China Normal University, Wuhan, Hubei 430079*
[13]*University of Illinois at Chicago, Chicago, Illinois 60607*
[14]*Chongqing University, Chongqing, 401331*
[15]*Creighton University, Omaha, Nebraska 68178*
[16]*Czech Technical University in Prague, FNSPE, Prague 115 19, Czech Republic*
[17]*Technische Universität Darmstadt, Darmstadt 64289, Germany*
[18]*National Institute of Technology Durgapur, Durgapur—713209, India*
[19]*ELTE Eötvös Loránd University, Budapest, Hungary H-1117*
[20]*Frankfurt Institute for Advanced Studies FIAS, Frankfurt 60438, Germany*
[21]*Fudan University, Shanghai, 200433*
[22]*Guangxi Normal University, Guilin, 541004*
[23]*University of Heidelberg, Heidelberg 69120, Germany*
[24]*University of Houston, Houston, Texas 77204*
[25]*Huzhou University, Huzhou, Zhejiang 313000*
[26]*Indian Institute of Science Education and Research (IISER), Berhampur 760010, India*
[27]*Indian Institute of Science Education and Research (IISER) Tirupati, Tirupati 517507, India*
[28]*Indian Institute Technology, Patna, Bihar 801106, India*
[29]*Indiana University, Bloomington, Indiana 47408*
[30]*Institute of Modern Physics, Chinese Academy of Sciences, Lanzhou, Gansu 730000*
[31]*University of Jammu, Jammu 180001, India*
[32]*Kent State University, Kent, Ohio 44242*
[33]*University of Kentucky, Lexington, Kentucky 40506-0055*
[34]*Lawrence Berkeley National Laboratory, Berkeley, California 94720*
[35]*Lehigh University, Bethlehem, Pennsylvania 18015*
[36]*Max-Planck-Institut für Physik, Munich 80805, Germany*
[37]*Michigan State University, East Lansing, Michigan 48824*
[38]*National Institute of Science Education and Research, HBNI, Jatni 752050, India*
[39]*National Cheng Kung University, Tainan 70101*
[40]*Nuclear Physics Institute of the CAS, Rez 250 68, Czech Republic*
[41]*The Ohio State University, Columbus, Ohio 43210*
[42]*Institute of Nuclear Physics PAN, Cracow 31-342, Poland*
[43]*Panjab University, Chandigarh 160014, India*
[44]*Purdue University, West Lafayette, Indiana 47907*
[45]*Rice University, Houston, Texas 77251*
[46]*Rutgers University, Piscataway, New Jersey 08854*
[47]*University of Science and Technology of China, Hefei, Anhui 230026*
[48]*South China Normal University, Guangzhou, Guangdong 510631*
[49]*Sejong University, Seoul, 05006, South Korea*
[50]*Shandong University, Qingdao, Shandong 266237*
[51]*Shanghai Institute of Applied Physics, Chinese Academy of Sciences, Shanghai 201800*
[52]*Southern Connecticut State University, New Haven, Connecticut 06515*
[53]*State University of New York, Stony Brook, New York 11794*
[54]*Instituto de Alta Investigación, Universidad de Tarapacá, Arica 1000000, Chile*
[55]*Temple University, Philadelphia, Pennsylvania 19122*
[56]*Texas A&M University, College Station, Texas 77843*
[57]*University of Texas, Austin, Texas 78712*
[58]*Tsinghua University, Beijing 100084*
[59]*University of Tsukuba, Tsukuba, Ibaraki 305-8571, Japan*
[60]*University of Chinese Academy of Sciences, Beijing, 101408*

^{61}United States Naval Academy, Annapolis, Maryland 21402
^{62}Valparaiso University, Valparaiso, Indiana 46383
^{63}Variable Energy Cyclotron Centre, Kolkata 700064, India
^{64}Warsaw University of Technology, Warsaw 00-661, Poland
^{65}Wayne State University, Detroit, Michigan 48201
^{66}Wuhan University of Science and Technology, Wuhan, Hubei 430065
^{67}Yale University, New Haven, Connecticut 06520
^{68}Indian Institute of Science Education and Research (IISER), Berhampur 760010, India

We report a measurement of exclusive J/ψ and $\psi(2s)$ photoproduction in Au + Au ultraperipheral collisions at $\sqrt{s_{\mathrm{NN}}} = 200$ GeV using the STAR detector. For the first time, (i) the $\psi(2s)$ photoproduction in midrapidity at the Relativistic Heavy-Ion Collider has been experimentally measured; (ii) nuclear suppression factors are measured for both the coherent and incoherent J/ψ production. At average photon-nucleon center-of-mass energy of 25.0 GeV, the coherent and incoherent J/ψ cross sections of Au nuclei are found to be $71 \pm 10\%$ and $36 \pm 7\%$, respectively, of that of free protons. The stronger suppression observed in the incoherent production provides a new experimental handle to study the initial-state parton density in heavy nuclei. Data are compared with theoretical models quantitatively.

The fundamental structure of protons and neutrons, collectively known as nucleons, is at the core of understanding modern physics. They are directly connected to problems of color confinement, the microscopic structures of visible matter, and the origin of dynamical mass generation from nonperturbative quantum chromodynamics (QCD). These problems are even more complex in the nuclear environment. Quark and gluon distributions for bound nucleons inside nuclei could be drastically different from those of the free nucleon. Understanding the fundamental structures of both nucleons and nuclei in a consistent framework is one of the most pressing tasks in high energy nuclear physics.

In recent years, vector meson photoproduction in ultraperipheral collisions (UPC) of heavy ions has provided an excellent experimental probe to study the structures of nucleons and nuclei [1]. Typically, these photon-induced interactions take place at a large impact parameter and only produce one particle, e.g., the J/ψ meson [2]. In this reaction, the target nucleus may stay intact (coherent) or break up (incoherent), largely depending on the momentum transfer of the interaction.

Specifically, coherent J/ψ photoproduction has been extensively investigated by heavy-ion collider experiments [3–12], where the resulting cross sections are found to be significantly suppressed with respect to those of a free proton [4,5,11–13]. Many models attempt to explain this phenomenon [14–19], but the underlying mechanism remains highly debated [1]. On the other hand, the nuclear suppression of incoherent vector meson production has never been explicitly measured. Comparing incoherent vector meson production on a heavy nucleus and on a free proton is equivalent to comparing the parton structure of bound and free nucleons. This is one of the most direct

and unambiguous approaches for studying bound nucleons in heavy-ion collisions.

In parallel to UPC measurements, hadronic proton-nucleus $(p + \mathrm{A})$ collision data have been an important experimental handle on the nuclear parton densities in heavy nuclei [20]. Despite a similar fundamental problem regarding the nuclear modification on parton distribution functions (nPDFs), UPC J/ψ and other vector mesons have the unique advantages of having little to no multiple parton interaction [21], no radiative energy loss [22], and a well-controlled event topology and environment. These effects, on the other hand, may complicate the interpretation of $p + \mathrm{A}$ data in terms of nPDFs [20], e.g., charged hadron production, heavy-flavor production, jet productions, etc. Therefore, UPC measurements in this Letter provide important and complementary data to the modification of nuclear parton densities in heavy nuclei. Although the hard scale of the UPC process is mainly determined by the vector meson mass (or more precisely the quark mass), the data of J/ψ and $\psi(2s)$ in this report provide a unique constraint on the nPDFs at the fixed scale. However, at the forthcoming Electron-Ion Collider, the precise control of the photon virtuality, thus an independent hard scale, will further improve the constraints of nPDFs from vector meson production.

In this Letter, we report measurements in Au + Au UPCs at $\sqrt{s_{\mathrm{NN}}} = 200$ GeV using the STAR detector at the Relativistic Heavy-Ion Collider (RHIC). Specifically, we measure: (i) coherent and incoherent J/ψ photoproduction cross sections on Au nuclei, associated with different neutron emission patterns as detected in zero degree calorimeters (ZDCs); (ii) photoproduction of $\psi(2s)$ at midrapidity; (iii) nuclear suppression factors with respect to free nucleons. The average photon-nucleon center-of-mass energy, $\langle W_{\gamma*\mathrm{N}} \rangle$, is approximately 25.0 GeV for

both coherent and incoherent processes at midrapidity in Au + Au UPCs [23]. The nuclear suppression data are compared with theoretical models: the nuclear shadowing model with leading twist approximation (LTA) [24,25] and the saturation model color glass condensate (CGC) [17,26].

The solenoidal tracker at the RHIC (STAR) detector [27] and its subsystems have been thoroughly described in previous STAR papers [28,29]. Charged particle tracking, including transverse momentum reconstruction and charge sign determination, is provided by the time projection chamber (TPC) [30] positioned in a 0.5 T solenoidal magnetic field. The TPC volume extends from 50 to 200 cm from the beam axis and covers pseudorapidities $|\eta| < 1.0$ over the full azimuthal angle, $0 < \phi < 2\pi$. The TPC also provides ionization loss (dE/dx) measurement of tracks used for particle identification. Surrounding the TPC is the barrel electromagnetic calorimeter (BEMC) [31], which is a lead-scintillator sampling calorimeter. The BEMC is segmented into 4800 optically isolated towers covering the full azimuthal angle for pseudorapidities $|\eta| < 1.0$. Between the TPC and BEMC is the time of flight (TOF) system. It is finely segmented in η and ϕ and provides fast trigger signals for charged particles in the range $|\eta| < 0.9$. There are two beam-beam counters (BBCs) [32], one on each side of the STAR main detector, covering a pseudorapidity range of $3.4 < |\eta| < 5.0$. There are also two ZDCs [27], 18 m along each beam direction covering $|\eta| > 6.7$, used to monitor the luminosity and to tag forward neutrons.

The UPC data were collected by the STAR experiment during the 2016 Au + Au run, which corresponds to an integrated luminosity of 13.5 nb^{-1} yielding approximately 2.4×10^7 UPC J/ψ triggered events. The J/ψ and $\psi(2s)$ candidates are reconstructed via the electron decay channel, $J/\psi(\psi(2s)) \to e^+e^-$. Based on this channel, the UPC J/ψ [$\psi(2s)$] trigger is defined by a topological selection of back-to-back clusters in the BEMC, a TOF charged track multiplicity between 2 and 6 (inclusive), and no BBC signal in either beam direction.

In the off-line analysis, the events are required to have a pair of tracks with a vertex that is reconstructed within 100 cm of the center of the STAR detector along the beam direction. Tracks are required to have at least 15 points (out of a maximum of 45) to ensure sufficient momentum resolution, contain no fewer than 11 points for the ionization energy loss determination to ensure good dE/dx resolution, and to be matched to a BEMC cluster for consistency with the trigger. Electron pair selection is performed based on the dE/dx of tracks, where the dominant contamination at $p_T \sim 1.5$ GeV/c is from pions. The variable $n_{\sigma,e}$ ($n_{\sigma,\pi}$) is the difference between the measured dE/dx value compared to an electron (π) hypothesis of the predicted dE/dx value. It is calculated in terms of the number of standard deviations from the predicted mean. The pair selection variable χ^2_{ee} is defined as

$n^2_{\sigma,e1} + n^2_{\sigma,e2}$ for tracks 1 and 2, and similarly for the π pair hypothesis. Tracks consistent with electron pairs were selected by requiring $\chi^2_{ee} < 10$ and those consistent with pion pairs were rejected by requiring $\chi^2_{ee} < \chi^2_{\pi\pi}$. The selections were performed separately for opposite-sign ($+-$) and like-sign ($++, --$) pairs. The like-sign pairs were taken as a measure of combinatoric backgrounds and subtracted from the opposite-sign pairs for final distributions.

Like-sign subtracted distributions of invariant mass m_{ee} and pair p_T were produced. Template distributions of signal J/ψ and background e^+e^- from quantum electrodynamics (QED) photon-photon interactions and $\psi(2S)$ production were also created. The templates used output from the STARlight [33] Monte Carlo program weighted by the H1 data [34], which were passed through the GEANT3-based [35] STAR detector simulation to model the detector response. To extract the J/ψ and $\psi(2s)$ yield, simultaneous fits of the templates to both the m_{ee} and pair p_T distributions were performed. For the differential cross section measurements in rapidity intervals, the same procedure was applied, and the J/ψ yields were extracted for both coherent and incoherent production. See the detailed procedure in Ref. [36].

The results were further divided into different neutron emission patterns as measured by the ZDCs, where neutrons can be produced by either the QED process of mutual Coulomb excitation [2] or nuclear breakup from hard scattering processes. The patterns of neutron emission are categorized as (i) $0n0n$—neither ZDC has detected a neutron; (ii) $0nXn$—one ZDC has detected at least one neutron and the other has no neutrons; (iii) $XnXn$—both ZDCs have detected at least one neutron. Results summing over these three categories are denoted as the *all n* category. Overlaps of ZDC hits from other events in the same RHIC bunch crossing caused migrations between these categories. This effect was measured in a sample of zero-bias data in terms of ZDC requirement, and the migrations were corrected for. This correction was up to 8% for the coherent J/ψ photoproduction cross section.

The differential cross section of J/ψ photoproduction as a function of p_T^2 and rapidity y is measured in the Au + Au UPCs as follows:

$$\frac{d^2\sigma}{dp_T^2 dy_i} = \frac{N_{\text{raw},i}}{\varepsilon_{\text{trig}} \, \text{corr}_i \, L \, \text{BR} \, \Delta p_{Ti}^2 \, 2\Delta y_i}. \quad (1)$$

Here $(d^2\sigma/dp_T^2 dy)_i$ is the doubly differential cross section in (p_T^2, y) bin i, where i is a single index that includes all measured (p_T^2, y) combinations. $N_{\text{raw},i}$ is the raw number of J/ψ in bin i. $\varepsilon_{\text{trig}}$ is an overall scale correction for trigger efficiency, and corr$_i$ is the acceptance and efficiency correction for bin i. The integrated luminosity is denoted by L, and BR = 5.97% is the branching ratio of J/ψ

decaying into an electron and positron [37]; Δp_{Ti}^2 and Δy_i are the widths of bin i. The factor of 2 is introduced because J/ψ events are measured within $|y| < 1$, while the cross section is only reported for $y > 0$; this factor is not included for the cross section $d\sigma/dy$ for $0nXn$ discussed later. The J/ψ acceptance corrections are based on the STARlight [33] MC events embedded into STAR zero-bias events, where a bin-by-bin unfolding technique is employed in the correction procedure as exhibited in Eq. (1).

For each rapidity of J/ψ there are two different contributions mixed together, a higher energy and a lower energy photon, which correspond to photons emitted by either nucleus. Based on the technique in Ref. [38], we resolve the photon energy ambiguity and measure the coherent J/ψ photoproduction cross section for $\gamma + \mathrm{Au} \to \mathrm{J}/\psi + \mathrm{Au}$. The details of this procedure are outlined in the companion article [36].

Different sources of systematic uncertainty on the differential cross section were investigated, which are similar to the previous STAR publication on J/ψ photoproduction in deuterons [39]. The $\psi(2s)$ production shares similar systematic uncertainties, except for the feed-down correction from $\psi(2s) \to J/\psi + X$. The background subtraction using fit templates introduces uncertainties from the fitting, resulting in 10%–20% on the background-subtracted distributions, depending on the J/ψ transverse momentum. Several factors contribute to the acceptance and efficiency corrections for pair mass and p_T distributions. The trigger efficiency determination results in final uncertainties $\sim$8%. The efficiency of matching tracks to BEMC energy deposits as measured with data has an uncertainty of $\sim$5% on the pair efficiency. The uncertainty on weighting of STARlight to match the p_T distributions is only significant on the steeply falling coherent J/ψ peak, where the pair detection efficiency uncertainty is up to 15%. The uncertainty from modeling radiative events in the simulation is $\sim$2% on pair acceptance. The background subtraction and acceptance uncertainties, including feed-down corrections and branching ratio, were determined bin by bin in mass and p_T of electron pairs. They were added in quadrature along with an overall 4% uncertainty on track and vertex reconstruction efficiency; this sum is shown with the displayed data points. The systematic uncertainty on modeling the transversely polarized photon flux is found to be up to 3.5% by varying the Au radius ± 0.5 fm, where the same method has been adopted as in Ref. [39]. Finally, there is an uncertainty of 10% on the luminosity measurement, which is the dominant systematic uncertainty source, resulting in a scale uncertainty of 10% on all cross sections, which is not displayed in the figures.

In Fig. 1, the differential cross sections $d\sigma/dy$ of J/ψ photoproduction as a function of $|y|$ for coherent (left) and incoherent (right) production are presented, for *all n* data and each neutron category separately. They are obtained by integrating the data over low (coherent) or
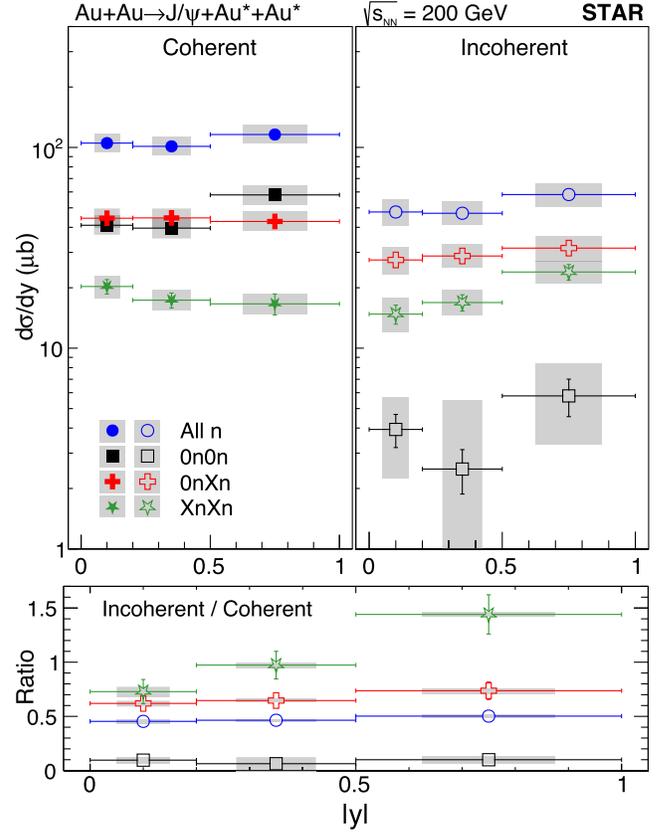

FIG. 1. Differential cross sections $d\sigma/dy$ for coherent (top left) and incoherent (top right) J/ψ photoproduction and their ratios (bottom) as a function of $|y|$ in $\mathrm{Au} + \mathrm{Au}$ UPCs at $\sqrt{s_{NN}} = 200$ GeV, for the different neutron categories defined in the text. Statistical uncertainties are represented by the error bars, and the systematic uncertainties are denoted as boxes. There is a systematic uncertainty on the cross sections of 10% from the integrated luminosity that is not shown.

high (incoherent) p_T^2 and using the template fits to correct to the full p_T^2 range [36]. The coherent spectra dominate for $p_T^2 < 0.02$ $(\mathrm{GeV}/c)^2$, while incoherent ones dominate the higher p_T^2. The rapidity interval includes both positive and negative rapidities, where the data are plotted at the bin center. The ratio between incoherent and coherent J/ψ production is also shown in the bottom panel. Note that the $0n0n$ in incoherent production is mostly dominated by non-neutron breakup from the target nucleus [40].

In Fig. 2, the first measurement of exclusive $\psi(2s)$ photoproduction has been reported at the top RHIC energy. The differential cross section $d\sigma/dy$ compares with that of the coherent J/ψ photoproduction and the STARLight model. The ratio between J/ψ and $\psi(2s)$ is shown in the bottom panel, where most systematic uncertainties are canceled. The ratio is found to be similar to the same measurement at 5.02 TeV at the LHC [9], and consistent with most models and data for pp or ep collisions [41–44]. Within the uncertainty of our measurement, we did not see any significantly different modification of $\psi(2s)$ relative to
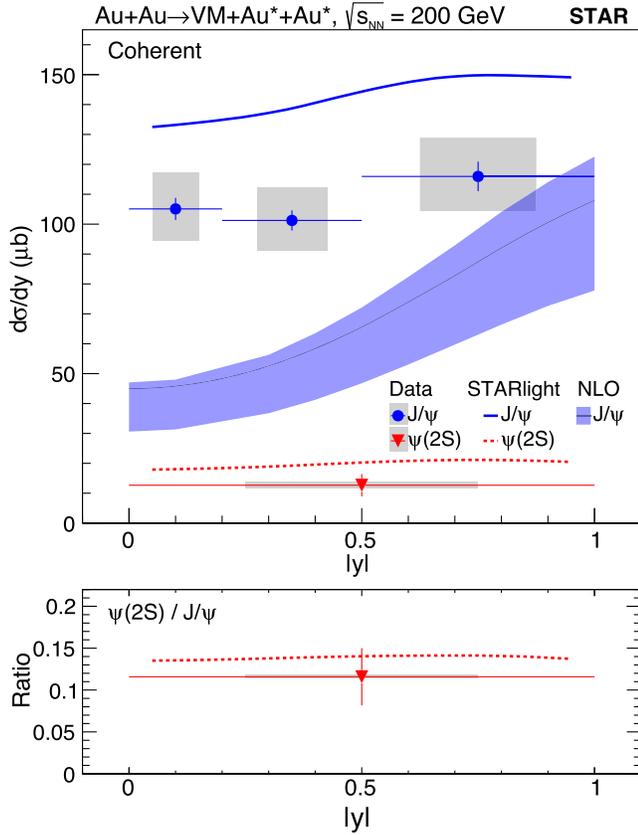
FIG. 2. Differential cross section $d\sigma/dy$ for coherent J/ψ and $\psi(2s)$ photoproduction as a function of $|y|$ in Au + Au UPCs at $\sqrt{s_{NN}} = 200$ GeV. The STARlight model [33] and the NLO pQCD calculations [46,47] are compared with the data. Ratio between $\psi(2s)$ and J/ψ is shown in the bottom panel. Statistical uncertainty is represented by the error bars, and the systematic uncertainty is denoted as boxes. There is a systematic uncertainty of 10% from the integrated luminosity that is not shown.

FIG. 3. Nuclear suppression factor of coherent (S_{coh}^{Au}, with respect to the impulse approximation) and incoherent (S_{incoh}^{Au}, with respect to the HERA data [34]) J/ψ photoproduction in Au + Au UPCs. The data are compared with the nuclear shadowing model [24] and the CGC model [17]. The CGC points are shifted from the vertical line for better visibility. Statistical uncertainties are represented by the error bars, and the systematic uncertainties are denoted as boxes. There is a systematic uncertainty of 10% from the integrated luminosity that is not shown.

J/ψ in Au + Au UPCs at RHIC energies with respect to free protons. Moreover, the colored band in Fig. 2 shows the first NLO perturbative QCD calculation of the J/ψ photoproduction at RHIC energies. The input nPDF is from EPPS21 [45], where the current uncertainty coming from the nPDF on the J/ψ production cross section can be as large as 50% to 160%. Consequently, this is not shown. The uncertainty band shown on the figure is only based on the scale uncertainty. For details, see Refs. [46,47]. This prediction has been found to be underestimated by more than a factor of 2 at midrapidity and 10%–20% at higher rapidity. These data will significantly constrain the nPDF at the NLO for both quarks and gluons.

In Fig. 3, the nuclear suppression factors of coherent (S_{coh}^{Au}) and incoherent (S_{incoh}^{Au}) J/ψ photoproduction are shown as a function of $\langle W_{\gamma^*N} \rangle$ in Au + Au UPCs. For the coherent case, the S_{coh}^{Au} is calculated based on the ratio between the coherent J/ψ cross section of *all n* and the impulse approximation (IA) [25], where IA represents the
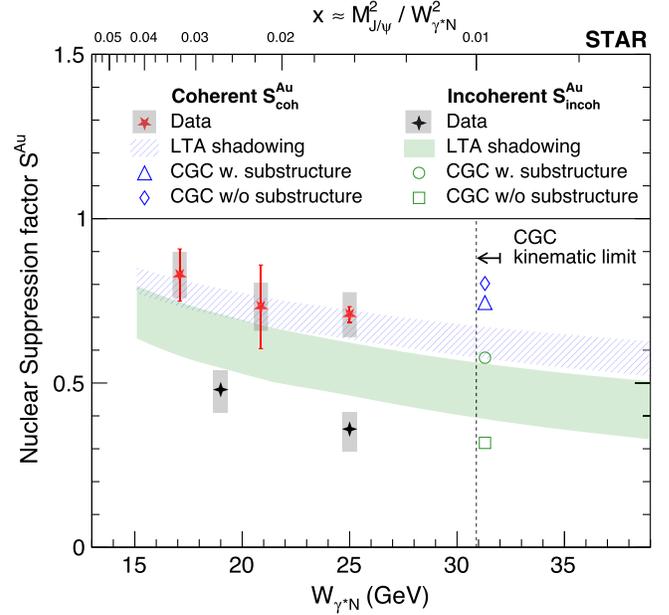
scenario without any nuclear effect constrained by free proton data [25]. The suppression factor at $\langle W_{\gamma^*N} \rangle = 25.0$ GeV is found to be $0.71 \pm 0.04 \pm 0.07 \pm 0.07$. The first quoted error is the model uncertainty on IA [25] for Au nuclei and the second error is a combination of statistics and systematic uncertainties added in quadrature, while the third is from the scale uncertainty of the integrated luminosity. Note that the data, LTA, and CGC calculations use the same IA calculation to ensure proper comparisons. Furthermore, since the estimate of IA of $\psi(2s)$ is less constrained than that of J/ψ [42], the corresponding nuclear suppression factor is not reported here.

For the incoherent suppression factor, S_{incoh}^{Au}, it is defined as the ratio between the incoherent J/ψ cross section of *all n* and the free proton data at HERA. In order to compare with photoproduction in ep collisions, we use the published H1 data and its well-constrained parametrization [34]. It is found that the STAR UPC incoherent p_T^2 distribution is well described by the H1 ep template, with a suppression factor found to be $0.36^{+0.03}_{-0.04} \pm 0.04 \pm 0.04$ at $\langle W_{\gamma^*N} \rangle = 25.0$ GeV. Here the first uncertainty is the H1 parametrization uncertainty, the second one is from the measurement that includes statistical and systematic uncertainty, and the third is the scale uncertainty on the integrated

luminosity. The details of this procedure, both for coherent and incoherent processes, are outlined in the companion article [36].

The nuclear shadowing model LTA and the saturation model CGC are compared with the data quantitatively. For the LTA, the upper bound of each band is showing the weak shadowing mode, while the lower bound shows the strong shadowing mode [24]. It is found that, for the first time, the incoherent suppression factor is less than that of the coherent production, as well as the strong shadowing mode in the LTA model. For the CGC model, although it is not strictly calculated at the STAR kinematic range due to the applicability of the model ($x > 0.01$, where x is the momentum fraction the parton carries of the nucleon), the incoherent data are found to be between the model scenarios calculated with or without subnucleonic fluctuation of the parton density [17]. Based on these data, it is hard to conclude if subnucleonic parton density fluctuation is present in the incoherent J/ψ photoproduction, contrary to the conclusion to a recent measurement by the ALICE Collaboration [48]. Note that the p_T^2 distributions of the incoherent production are found to be consistent between STAR and ALICE. Nevertheless, the reported data provide new insights to the nuclear suppression in both coherent and incoherent J/ψ photoproduction, where incoherent production is found to be more suppressed than the coherent counterparts. Within the model of LTA and other models that are based on nuclear PDFs, this new data will significantly constrain the quantitative description of nuclear parton densities in heavy nuclei, complementary to other measurements in $p + A$ collisions.

In conclusion, differential cross sections of J/ψ photo-production in coherent and incoherent processes as a function of rapidity y and the first measurement of photoproduction of $\psi(2s)$ in Au + Au UPCs at $\sqrt{s_{NN}} = 200$ GeV have been reported. These cross sections are measured separately in different neutron emission categories, as detected by the zero degree calorimeters. The relative coherent cross section to that of a free nucleon is found to be $71 \pm 10\%$ ($\sim 30\%$ suppressed). The incoherent J/ψ photoproduction has been compared to that of a free proton based on the H1 data, where a stronger suppression than that of the coherent production is observed with a relative cross section of $36 \pm 7\%$ ($\sim 60\%$ suppressed). This is stronger than predictions from the nuclear shadowing model, and does not directly support the CGC model with subnucleonic fluctuation. The parton density at the top RHIC energy lies in the transition region ($x_{parton} \sim 0.01$) between large momentum quarks ($x_{parton} > 0.1$) and low momentum gluons ($x_{parton} < 0.001$), which is essential to the understanding of both gluon saturation and nuclear shadowing mechanisms. This measurement provides important constraints to the parton density and is an essential experimental baseline for such measurements at the upcoming Electron-Ion Collider.

[1] M. Arslandok *et al.*, Hot QCD white paper, arXiv:2303 .17254.

[2] C. A. Bertulani, S. R. Klein, and J. Nystrand, Physics of ultra-peripheral nuclear collisions, Annu. Rev. Nucl. Part. Sci. **55**, 271 (2005).

[3] S. Afanasiev *et al.* (PHENIX Collaboration), Photoproduction of J/ψ and of high mass e^+e^- in ultra-peripheral Au + Au collisions at $\sqrt{s_{NN}} = 200$ GeV, Phys. Lett. B **679**, 321 (2009).

[4] V. Khachatryan *et al.* (CMS Collaboration), Coherent J/ψ photoproduction in ultra-peripheral PbPb collisions at $\sqrt{s_{NN}} = 2.76$ TeV with the CMS experiment, Phys. Lett. B **772**, 489 (2017).

[5] B. Abelev *et al.* (ALICE Collaboration), Coherent J/ψ photoproduction in ultra-peripheral Pb-Pb collisions at $\sqrt{s_{NN}} = 2.76$ TeV, Phys. Lett. B **718**, 1273 (2013).

[6] S. Acharya *et al.* (ALICE Collaboration), Coherent photoproduction of ρ^0 vector mesons in ultra-peripheral Pb-Pb collisions at $\sqrt{s_{NN}} = 5.02$ TeV, J. High Energy Phys. 06 (2020) 035.

[7] S. Acharya *et al.* (ALICE Collaboration), First measurement of coherent $\rho 0$ photoproduction in ultra-peripheral Xe–Xe collisions at $\sqrt{s_{NN}} = 5.44$ TeV, Phys. Lett. B **820**, 136481 (2021).

[8] S. Acharya *et al.* (ALICE Collaboration), First measurement of the $|t|$-dependence of coherent J/ψ photonuclear production, Phys. Lett. B **817**, 136280 (2021).

[9] S. Acharya *et al.* (ALICE Collaboration), Coherent J/ψ and ψ' photoproduction at midrapidity in ultra-peripheral Pb-Pb

collisions at $\sqrt{s_{NN}}$ = 5.02 TeV, Eur. Phys. J. C **81**, 712 (2021).

[10] R. Aaij *et al.* (LHCb Collaboration), J/ψ photoproduction in Pb-Pb peripheral collisions at $\sqrt{s_{NN}}$ = 5 TeV, Phys. Rev. C **105**, L032201 (2022).

[11] A. Tumasyan *et al.* (CMS Collaboration), Probing small Bjorken-x nuclear gluonic structure via coherent J/ψ photoproduction in ultraperipheral PbPb collisions at $\sqrt{s_{NN}}$ = 5.02 TeV, Phys. Rev. Lett. **131**, 262301 (2023).

[12] S. Acharya *et al.* (ALICE Collaboration), Energy dependence of coherent photonuclear production of J/ψ mesons in ultra-peripheral Pb-Pb collisions at $\sqrt{s_{NN}}$ = 5.02 TeV, J. High Energy Phys. 10 (2023) 119.

[13] B. Abelev *et al.* (ALICE Collaboration), Coherent J/ψ photoproduction in ultra-peripheral Pb-Pb collisions at $\sqrt{s_{NN}}$ = 2.76 TeV, Phys. Lett. B **718**, 1273 (2013).

[14] M. Alvioli, L. Frankfurt, V. Guzey, M. Strikman, and M. Zhalov, Color fluctuation phenomena in γA collisions at the LHC, CERN Proc. **1**, 151 (2018).

[15] V. Guzey and M. Zhalov, Exclusive J/ψ production in ultraperipheral collisions at the LHC: Constrains on the gluon distributions in the proton and nuclei, J. High Energy Phys. 10 (2013) 207.

[16] V. Guzey, M. Strikman, and M. Zhalov, Nucleon dissociation and incoherent J/ψ photoproduction on nuclei in ion ultraperipheral collisions at the Large Hadron Collider, Phys. Rev. C **99**, 015201 (2019).

[17] H. Mäntysaari, F. Salazar, and B. Schenke, Nuclear geometry at high energy from exclusive vector meson production, Phys. Rev. D **106**, 074019 (2022).

[18] B. Sambasivam, T. Toll, and T. Ullrich, Investigating saturation effects in ultraperipheral collisions at the LHC with the color dipole model, Phys. Lett. B **803**, 135277 (2020).

[19] T. Toll and T. Ullrich, Exclusive diffractive processes in electron-ion collisions, Phys. Rev. C **87**, 024913 (2013).

[20] N. Armesto, Small collision systems: Theory overview on cold nuclear matter effects, EPJ Web Conf. **171**, 11001 (2018).

[21] T. Sjöstrand, The development of MPI modeling in Pythia, Adv. Ser. Dir. High Energy Phys. **29**, 191 (2018).

[22] F. Arleo, G. Jackson, and S. Peigné, Impact of fully coherent energy loss on heavy meson production in pA collisions, J. High Energy Phys. 01 (2022) 164.

[23] Note that there is a -0.5 GeV shift in the estimate of $\langle W_{\gamma^*N} \rangle$ at midrapidity $|y| < 0.2$, caused by the higher photon flux of the lower energy photon contribution; however, the effect of this shift is found to be negligible.

[24] E. Kryshen, M. Strikman, and M. Zhalov, Photoproduction of J/ψ with neutron tagging in ultra-peripheral collisions of nuclei at RHIC and the LHC, Phys. Rev. C **108**, 024904 (2023).

[25] V. Guzey, E. Kryshen, M. Strikman, and M. Zhalov, Evidence for nuclear gluon shadowing from the ALICE measurements of PbPb ultraperipheral exclusive J/ψ production, Phys. Lett. B **726**, 290 (2013).

[26] H. Mäntysaari and B. Schenke, Evidence of strong proton shape fluctuations from incoherent diffraction, Phys. Rev. Lett. **117**, 052301 (2016).

[27] K. H. Ackermann *et al.* (STAR Collaboration), STAR detector overview, Nucl. Instrum. Methods Phys. Res., Sect. A **499**, 624 (2003).

[28] J. Adam *et al.* (STAR Collaboration), Low-p_T e^+e^- pair production in Au + Au collisions at $\sqrt{s_{NN}}$ = 200 GeV and U + U collisions at $\sqrt{s_{NN}}$ = 193 GeV at STAR, Phys. Rev. Lett. **121**, 132301 (2018).

[29] J. Adam *et al.* (STAR Collaboration), Measurements of W and Z/γ^* cross sections and their ratios in p + p collisions at RHIC, Phys. Rev. D **103**, 012001 (2021).

[30] M. Anderson *et al.*, The star time projection chamber: A unique tool for studying high multiplicity events at RHIC, Nucl. Instrum. Methods Phys. Res., Sect. A **499**, 659 (2003).

[31] M. Beddo *et al.* (STAR Collaboration), The STAR barrel electromagnetic calorimeter, Nucl. Instrum. Methods Phys. Res., Sect. A **499**, 725 (2003).

[32] C. A. Whitten (STAR Collaboration), The beam-beam counter: A local polarimeter at STAR, AIP Conf. Proc. **980**, 390 (2008).

[33] S. R. Klein, J. Nystrand, J. Seger, Y. Gorbunov, and J. Butterworth, STARlight: A Monte Carlo simulation program for ultra-peripheral collisions of relativistic ions, Comput. Phys. Commun. **212**, 258 (2017).

[34] C. Alexa *et al.* (H1 Collaboration), Elastic and proton-dissociative photoproduction of J/ψ mesons at HERA, Eur. Phys. J. C **73**, 2466 (2013).

[35] R. Brun, F. Bruyant, M. Maire, A. C. McPherson, and P. Zanarini, GEANT3, CERN-DD-EE-84-01, https://cds.cern.ch/record/1119728 (1987).

[36] M. I. Abdulhamid *et al.* (STAR Collaboration), companion paper, Exclusive J/ψ, $\psi(2s)$, and e^+e^- pair production in Au + Au ultraperipheral collisions at the BNL Relativistic Heavy Ion Collider, Phys. Rev. C **110**, 014911 (2024).

[37] P. A. Zyla *et al.* (Particle Data Group), Review of particle physics, Prog. Theor. Exp. Phys. **2020**, 083C01 (2020).

[38] V. Guzey, M. Strikman, and M. Zhalov, Disentangling coherent and incoherent quasielastic J/ψ photoproduction on nuclei by neutron tagging in ultraperipheral ion collisions at the LHC, Eur. Phys. J. C **74**, 2942 (2014).

[39] M. Abdallah *et al.* (STAR Collaboration), Probing the gluonic structure of the deuteron with J/ψ photoproduction in d + Au ultraperipheral collisions, Phys. Rev. Lett. **128**, 122303 (2022).

[40] W. Chang, E.-C. Aschenauer, M. D. Baker, A. Jentsch, J.-H. Lee, Z. Tu, Z. Yin, and L. Zheng, Investigation of the background in coherent J/ψ production at the EIC, Phys. Rev. D **104**, 114030 (2021).

[41] M. B. Gay Ducati, M. T. Griep, and M. V. T. Machado, Diffractive photoproduction of radially excited psi(2S) mesons in photon-Pomeron reactions in PbPb collisions at the CERN LHC, Phys. Rev. C **88**, 014910 (2013).

[42] C. Adloff *et al.* (H1 Collaboration), Diffractive photoproduction of psi(2S) mesons at HERA, Phys. Lett. B **541**, 251 (2002).

[43] T. Aaltonen *et al.* (CDF Collaboration), Observation of exclusive charmonium production and $\gamma + \gamma$ to $\mu^+\mu^-$ in $p\bar{p}$ collisions at $\sqrt{s}$ = 1.96 TeV, Phys. Rev. Lett. **102**, 242001 (2009).

[44] R. Aaij *et al.* (LHCb Collaboration), Updated measurements of exclusive J/ψ and $\psi(2S)$ production cross-sections in pp collisions at $\sqrt{s} = 7$ TeV, J. Phys. G **41,** 055002 (2014).

[45] K. J. Eskola, P. Paakkinen, H. Paukkunen, and C. A. Salgado, Towards EPPS21 nuclear PDFs, SciPost Phys. Proc. **8,** 033 (2022).

[46] K. J. Eskola, C. A. Flett, V. Guzey, T. Löytäinen, and H. Paukkunen, Next-to-leading order perturbative QCD predictions for exclusive J/ψ photoproduction in oxygen-oxygen and lead-lead collisions at energies available at the CERN Large Hadron Collider, Phys. Rev. C **107,** 044912 (2023).

[47] K. J. Eskola, C. A. Flett, V. Guzey, T. Löytäinen, and H. Paukkunen, Exclusive J/ψ photoproduction in ultraperipheral Pb + Pb collisions at the CERN Large Hadron Collider calculated at next-to-leading order perturbative QCD, Phys. Rev. C **106,** 035202 (2022).

[48] S. Acharya *et al.* (ALICE Collaboration), First measurement of the $|t|$-dependence of incoherent J/ψ photonuclear production, Phys. Rev. Lett. **132,** 162302 (2024).